Supplementary Information: Propagation of THz magnons in a one-dimensional transition metal decorated holey graphyne strip with tunable bandgaps

Prabin Pyakurel Sharma, Chaithanya Purushottam Bhat, and Debashis Bandyopadhyay*
Department of Physics, Birla Institute of Technology and Science Pilani, Rajasthan 333031, India

I Optimized structures of transition-metal (V, Cr, Mn, Fe, Co, Ni) adatom functionalized holey graphyne strip with first principles method: top and side view

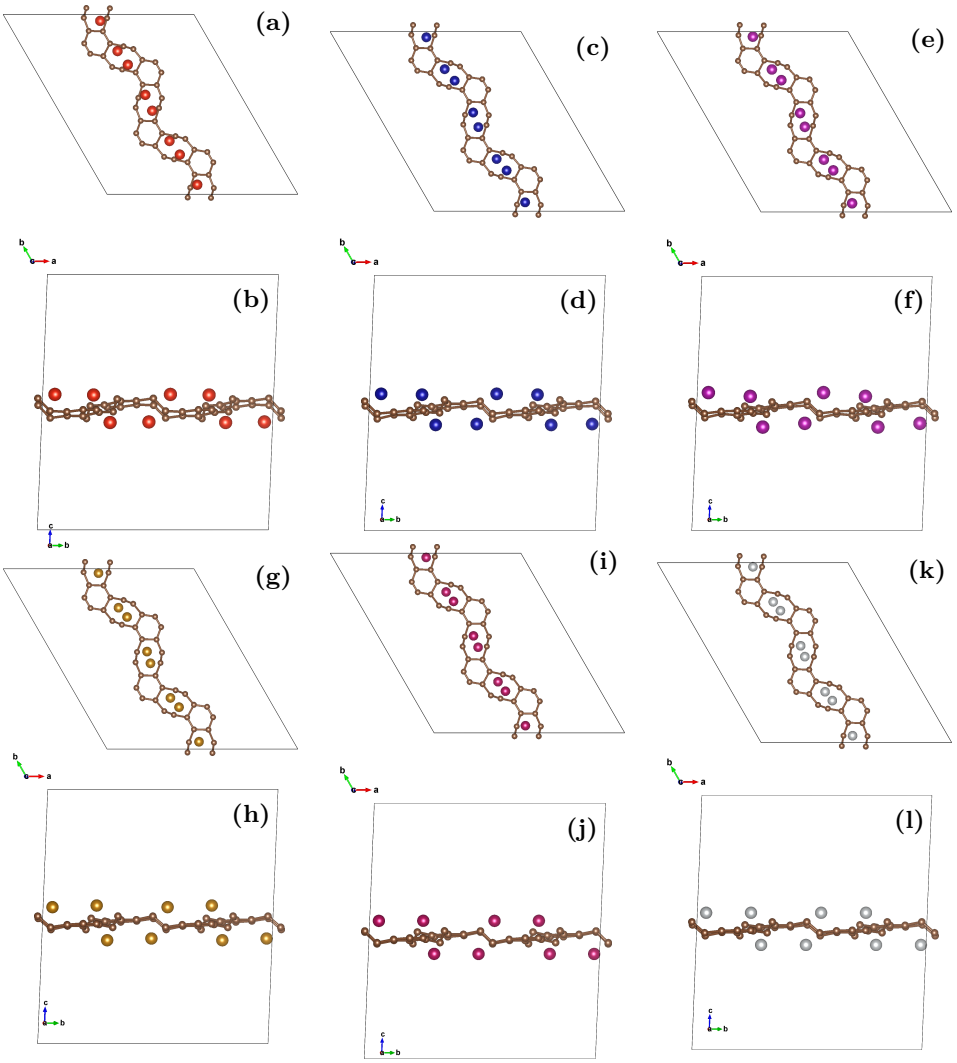

SI Figure 1. Top- and side-view configurations for V (a,b), Cr (c,d), Mn (e,f), Fe (g,h), Co (i,j), and Ni (k,l) adatoms on the surface. All systems show essentially the same adsorption geometry, with only minor differences in the distance between each transition-metal adatom and its nearest carbon atoms.

* bandy@pilani.bits-pilani.ac.in

II Molecular dynamics and structural stability

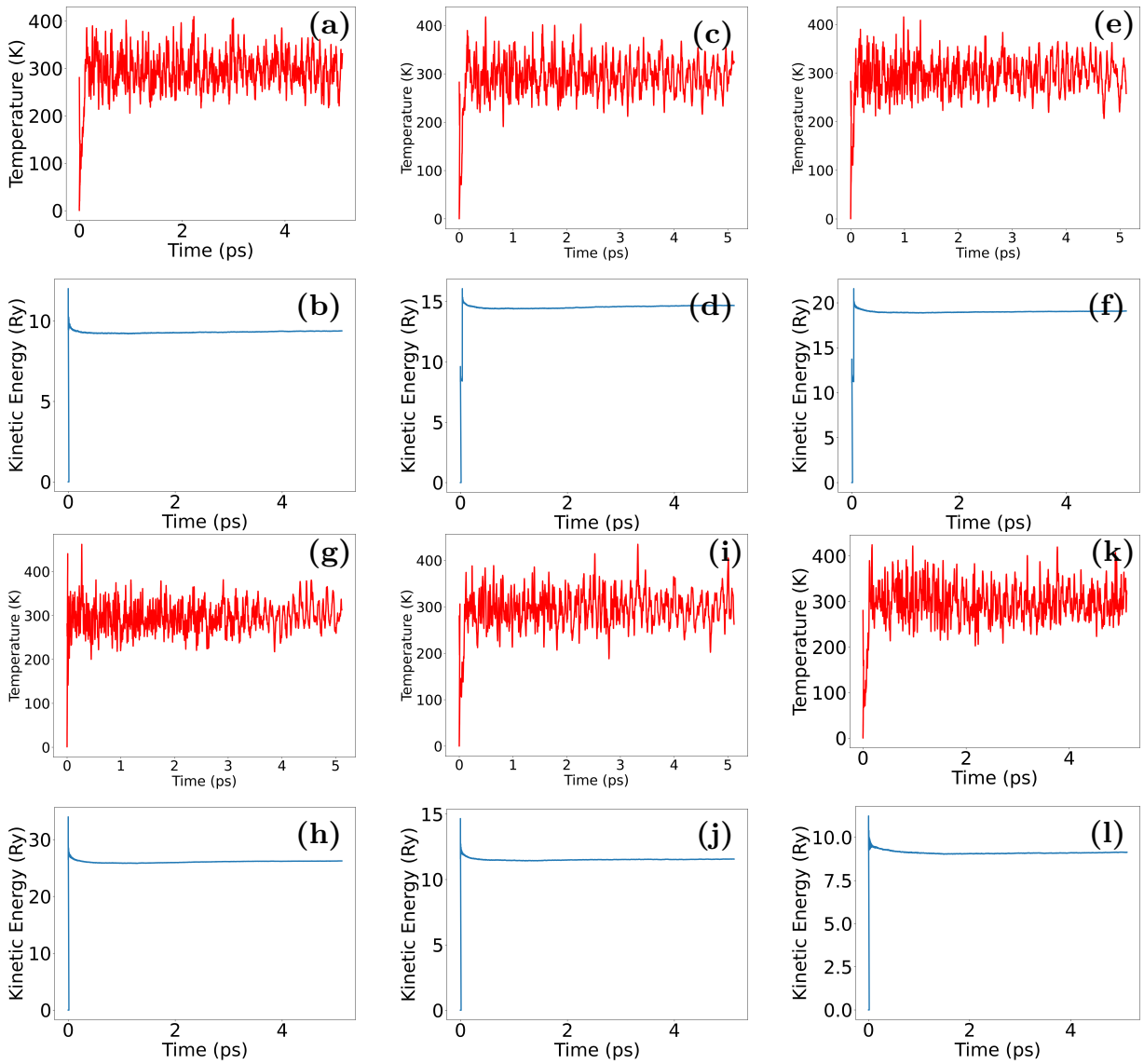

SI Figure 2. Panels (a, c, e, g, i, k) (top row) display the temperature regulation during molecular dynamics simulations for the adatoms: V, Cr, Mn, Fe, Co, and Ni, respectively, while panels (b, d, f, h, j, l) (bottom row) present the corresponding electronic kinetic energy profiles for V, Cr, Mn, Fe, Co, and Ni, respectively.

The results confirm that five systems (V, Cr, Fe, Mn, and Co) reach stable equilibration under the NVT ensemble at 300 K using the Nosé–Hoover thermostat. The electronic kinetic energy and temperature plots show that initial fluctuations subside as the systems equilibrate. For Ni, however, the transition metal atoms drift away from the strip at room temperature. The steady mean bond lengths from Figure 3 show that the structures are stable at 300 K. The systems with Mn, Fe, and Co adatoms seem to be the most stable, as there are no drifts in the bond lengths.

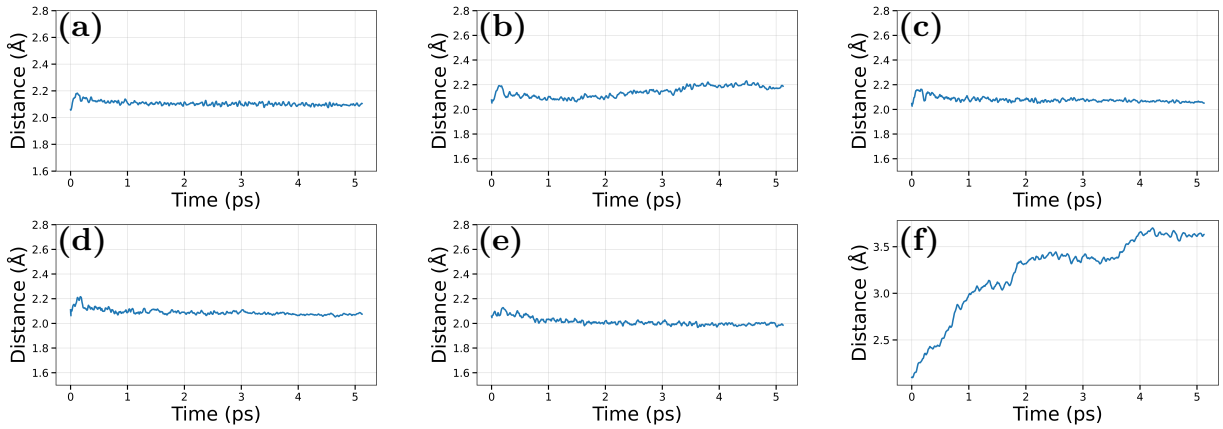

SI Figure 3. The average bond lengths of the TM-C bond fluctuating during the MD simulation for the TM adatoms: a) V, b) Cr, c) Mn, d) Fe, e) Co, f) Ni.

III Linear Spin Wave Theory Derivation

This section details the analytical derivation of the magnon spectrum for the 8-sublattice holey graphyne system. We employ Linear Spin Wave Theory (LSWT) following the generalized formalism by Toth and Lake [1] for non-Bravais lattices to numerically find the ground state and solve the dispersion relation for our systems.

The system is described by a Heisenberg Hamiltonian including a Zeeman coupling to an external magnetic field. We adopt the convention that a positive exchange constant J_{ij} favors ferromagnetic alignment, and we write

$$\mathcal{H} = -\sum_{\langle i,j \rangle} J_{ij} \mathbf{S}_i \cdot \mathbf{S}_j - g\mu_B \sum_i \mathbf{B} \cdot \mathbf{S}_i. \tag{1}$$

Here, indices i, j run over magnetic sites, and spin magnitudes S_i are treated as site-dependent variables. A positive $J_{ij} > 0$ denotes ferromagnetic interaction, while $J_{ij} < 0$ denotes antiferromagnetic interaction.

To treat general magnetic orders, we define a local coordinate frame (x', y', z') for each site i, where z'_i aligns with the classical spin direction, which already includes any canting induced by the external magnetic field. The global spin operators relate to the local frame via $\mathbf{S}_i = R_i \mathbf{S}'_i$.

We bosonize the local spin operators using the Holstein–Primakoff approximation. To linear order in $1/S$, the transformations are

$$S'^z_i = S_i - a^\dagger_i a_i, \tag{2}$$

$$S'^+_i \approx \sqrt{2S_i}\, a_i, \tag{3}$$

$$S'^-_i \approx \sqrt{2S_i}\, a^\dagger_i. \tag{4}$$

Substituting these into the rotated Hamiltonian and retaining terms quadratic in boson operators yields:

$$\mathcal{H}^{(2)} = \sum_{i,j} \left[A_{ij} a^\dagger_i a_j + \frac{1}{2} B_{ij} \left(a_i a_j + a^\dagger_i a^\dagger_j \right) \right], \tag{5}$$

where the Zeeman term contributes only to the diagonal elements A_{ii} and produces a uniform shift of the magnon energies. Terms proportional to A_{ij} preserve magnon number (hopping), while B_{ij} terms create or annihilate magnon pairs, arising specifically from antiferromagnetic components.

We perform a Fourier transform for sublattice μ in unit cell n, defined as

$$a_{n,\mu} = N^{-1/2} \sum_{\mathbf{k}} e^{-i\mathbf{k}\cdot\mathbf{r}_{n,\mu}} b_{\mathbf{k},\mu}. \tag{6}$$

The Hamiltonian in momentum space becomes

$$\mathcal{H}_{LSWT} = \sum_{\mathbf{k}} \Psi^\dagger_{\mathbf{k}} D(\mathbf{k}) \Psi_{\mathbf{k}}, \tag{7}$$

using the basis

$$\Psi_{\mathbf{k}} = \left(b_{\mathbf{k},1}, \ldots, b_{\mathbf{k},8}, b^{\dagger}_{-\mathbf{k},1}, \ldots, b^{\dagger}_{-\mathbf{k},8}\right)^{T}. \tag{8}$$

The 16×16 dynamical matrix $D(\mathbf{k})$ takes the block form:

$$D(\mathbf{k}) = \begin{pmatrix} \mathbf{A}(\mathbf{k}) & \mathbf{B}(\mathbf{k}) \\ \mathbf{B}^{\dagger}(\mathbf{k}) & \mathbf{A}^{*}(\mathbf{k}) \end{pmatrix}. \tag{9}$$

The diagonal elements

$$A_{\mu\mu} = \sum_{\nu} J_{\mu\nu} S_{\nu} \cos\left(\phi_{\mu\nu}\right) + g\mu_B \mathbf{B} \cdot \hat{z}'_{\mu} \tag{10}$$

represent the molecular field energy. The second term originates from the Zeeman coupling and lifts the Goldstone mode at finite magnetic field. The off-diagonal elements depend on the specific bond type:

- **Ferromagnetic ($J_{ij} > 0$):** $A_{\mu\nu}(\mathbf{k}) = -J_{\mu\nu}\sqrt{S_{\mu}S_{\nu}}e^{i\mathbf{k}\cdot\mathbf{d}_{\mu\nu}}$, and $B_{\mu\nu} = 0$.
- **Antiferromagnetic ($J_{ij} < 0$):** $A_{\mu\nu} = 0$ and $B_{\mu\nu}(\mathbf{k}) = -J_{\mu\nu}\sqrt{S_{\mu}S_{\nu}}e^{i\mathbf{k}\cdot\mathbf{d}_{\mu\nu}}$.

Given the specific connectivity of the holey graphyne lattice, the non-zero matrix elements populating the off-diagonal blocks are summarized in Table 1.

Table I. Non-zero dynamical matrix elements determined by the holey graphyne lattice connectivity.

Bond Pair (i,j)	**Matrix Elements**	**Interaction**
(1,3)	$A_{13}, A_{31}, B_{13}, B_{31}$	J_{1-3}
(1,7)	$A_{17}, A_{71}, B_{17}, B_{71}$	J_{1-7}
(2,4)	$A_{24}, A_{42}, B_{24}, B_{42}$	J_{2-4}
(2,8)	$A_{28}, A_{82}, B_{28}, B_{82}$	J_{2-8}
(3,5)	$A_{35}, A_{53}, B_{35}, B_{53}$	J_{3-5}
(4,6)	$A_{46}, A_{64}, B_{46}, B_{64}$	J_{4-6}
(5,8)	$A_{58}, A_{85}, B_{58}, B_{85}$	J_{5-8}
(6,7)	$A_{67}, A_{76}, B_{67}, B_{76}$	J_{6-7}

The magnon dispersion relations $\omega_{\mathbf{k}}$ are finally obtained by numerically solving the generalized eigenvalue problem

$$gD(\mathbf{k})\mathbf{v}_{\mathbf{k}} = \omega_{\mathbf{k}}\mathbf{v}_{\mathbf{k}}, \tag{11}$$

with metric tensor $g = \mathrm{diag}(\mathbf{1}_{8\times8}, -\mathbf{1}_{8\times8})$.

IV Dependence of exchange interaction on distance

The exchange interaction parameters were obtained using the TB2J package. The strongest interactions were found between the nearest-neighbour atoms, as illustrated in SI Figure 4. With increasing interatomic distance, the exchange interactions decay rapidly and approach zero.

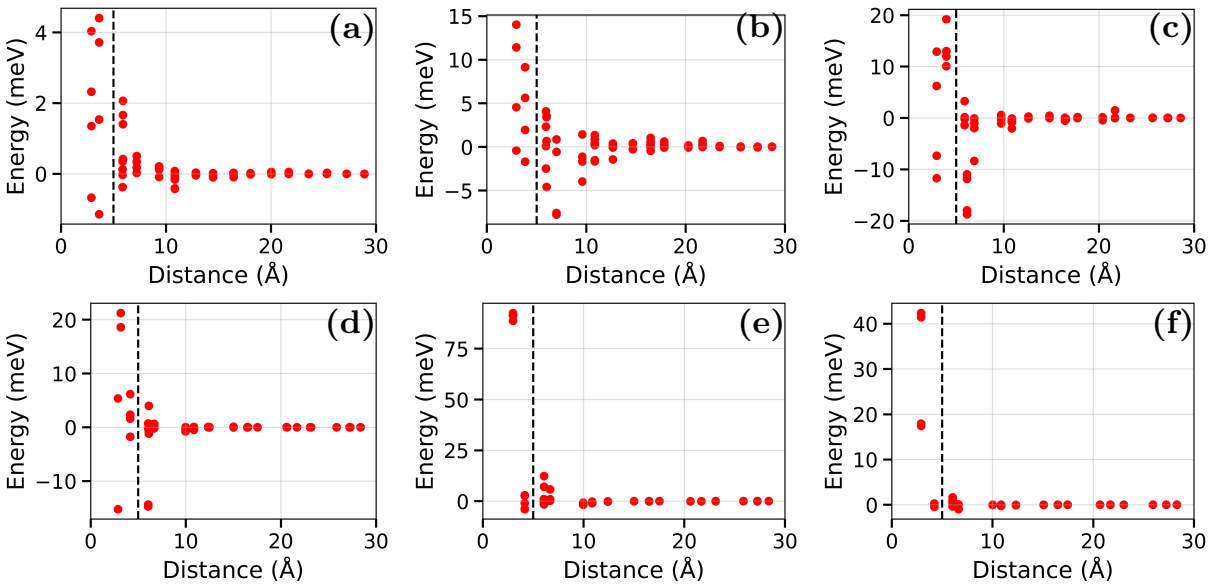

SI Figure 4. Calculated exchange interaction J_{ij} as a function of interatomic distance R_{ij} for transition metals (V, Cr, Mn, Fe, Co, and Ni). Only the nearest-neighbour exchange interactions were considered in the analysis, corresponding to the data points on the left of the dashed vertical line in each plot.

[1] S. Toth and B. Lake, Journal of Physics: Condensed Matter **27**, 166002 (2015).